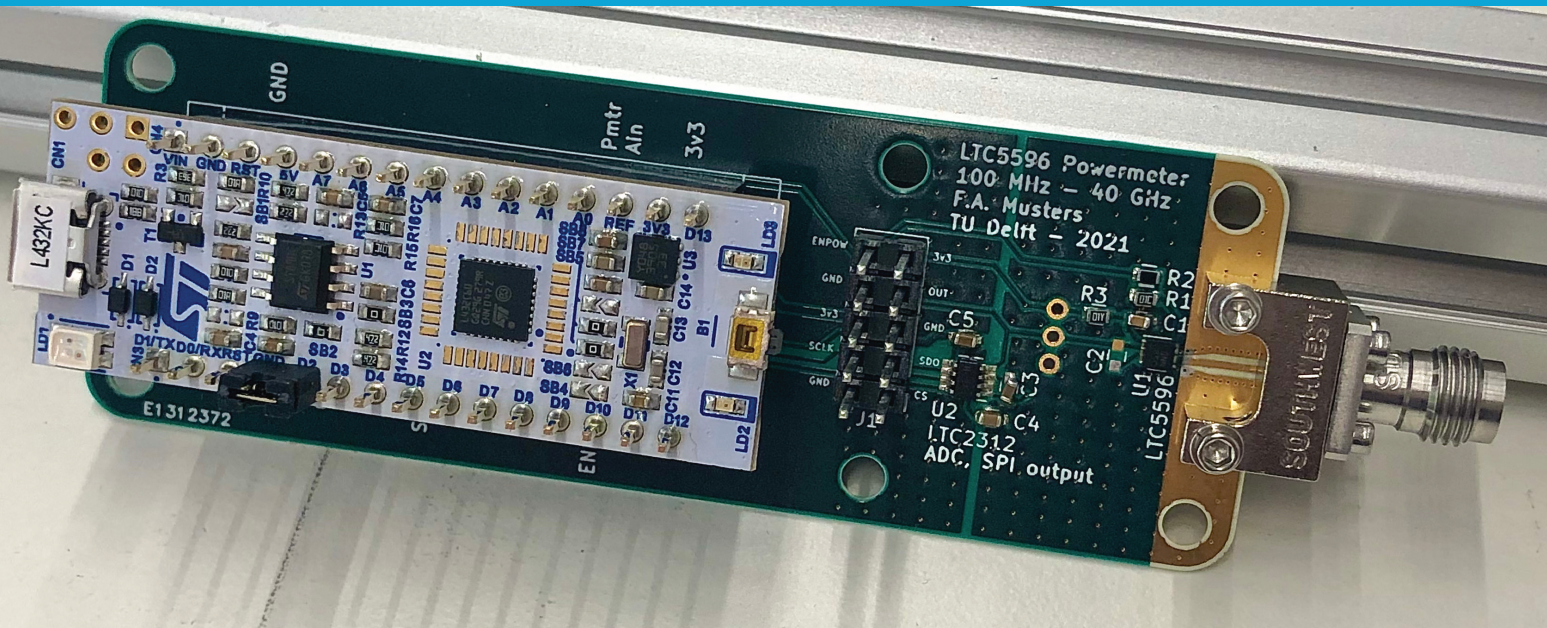


# Uncertainty of a RMS Power Detector

Subproject within  
the ADome project





# Uncertainty of an RMS powermeter

by

H. D. Denekamp,  
J. G. Gilcher

to obtain the degree of Bachelor of Science  
at the Delft University of Technology,

Project duration: April 19, 2021 – June 18, 2021

Thesis committee: Dr. M. Spirito, Associate Professor, ELCA, TU Delft, supervisor  
Prof. K. Makinwa, Professor, EI, TU Delft  
Dr. M. Alonso-delPino, Assistant Professor, THZ, TU Delft  
MSc. F. Musters, TU Delft, supervisor



# Abstract

The accuracy of a true-RMS detector board based on the Analog Devices LTC5596 is determined by measuring the input power and the output voltage. A number of samples of the output voltage is taken and the mean and standard deviation is shown. These measurements are done for single-tone excitation with a direct connection and over-the-air setup, and for multi-tone excitation with a direct connection.

It has been demonstrated that the detector response worsens with over-the-air excitation, resulting in a doubling of the standard deviation in the output voltage compared to a direct connection. With multi-tone excitation, the standard deviation is fifteen times higher than with a direct connection. Additionally, with multi-tone excitation the mean output voltage is lower than with the same input power as single-tone. This discrepancy increases with the amount of tones.

A Keysight Advanced Design System simulation is also presented for the three different measurement setups. With the use of a Monte Carlo simulation uncertainty bounds between the function generator and the power detector are made. Furthermore the noise of the power detector is simulated and sources of noise analyzed.



# Preface

This project was carried out in the context of a Bachelor graduation project, as part of a group that worked on improving different aspects of the ADome antenna measurement system. The group worked in these projects for one quarter, about eight weeks.

Our project concerned the characterization of the power detector of the ADome. However, as the amount of laboratory access was unknown before starting the project and due to personal circumstances of one of the group members, part of the work was shifted to creating a simulation testbench of the measurement setups. In working on these measurements, we feel the project has been very valuable in improving our understanding of RF work in a more practical environment and also increasing our proficiency with the electronic design software, Keysight ADS.

We would like to thank our supervisors Marco Spirito, Ferry Muster and Richard Coesoij for their guidance during the project. We would also like to thank our group members Daan Roos, Tycho van Velden, Alexander Becoy and Remy Zhang for the support during the project.

*David Denekamp and Jakob Gilcher  
Delft, January 2021*



# Contents

<b>Abstract</b>	<b>iii</b>
<b>1 Introduction</b>	<b>1</b>
1.1 Background on the ADome . . . . .	1
1.2 ADome Subprojects . . . . .	1
1.3 Problem Statement . . . . .	2
1.4 <i>State of the Art</i> Analysis . . . . .	3
1.5 Thesis Structure . . . . .	3
<b>2 Programme of Requirements</b>	<b>5</b>
2.1 Measurement Setup and Results . . . . .	5
2.2 Simulation. . . . .	5
<b>3 Measurement Setups</b>	<b>7</b>
3.1 Continuous Wave Direct Connection . . . . .	7
3.1.1 The Power Detector Board. . . . .	7
3.1.2 Function Generator. . . . .	9
3.1.3 Spectrum Analyzer . . . . .	9
3.1.4 The Cables . . . . .	11
3.1.5 The Power Divider . . . . .	11
3.2 Continuous Wave Direct Connection OTA . . . . .	11
3.2.1 Amplifier. . . . .	12
3.2.2 The antenna and free space loss . . . . .	12
3.3 Multi-tone Direct Connection. . . . .	13
3.3.1 IQ Mixer. . . . .	13
3.3.2 The Pre-Mixer Amplifier . . . . .	13
3.3.3 The DAC . . . . .	14
3.4 Software Setup . . . . .	14
<b>4 Simulation</b>	<b>17</b>
4.1 Continuous Wave Direct Connection Setup. . . . .	17
4.1.1 Equipment . . . . .	17
4.1.2 Noise Simulation . . . . .	19
4.1.3 Comparison Power Detector and Spectrum Analyzer with Monte Carlo. . . . .	21
4.2 Continuous Wave Over-th-Air Setup. . . . .	23
4.2.1 Equipment . . . . .	24
4.2.2 Noise Simulation Results. . . . .	24
4.2.3 Simulation Check with Measurements . . . . .	25
4.3 Multi-tone Direct Connection. . . . .	26
4.3.1 Equipment . . . . .	26
4.3.2 Noise Simulation . . . . .	26
4.3.3 Uncertainty Bound Results. . . . .	27
<b>5 Measurement Results</b>	<b>29</b>
5.1 Direct Connection . . . . .	29
5.2 Over-the-Air Setup . . . . .	31
5.3 Multi-tone Setup . . . . .	31

---

<b>6 Discussion and Conclusion</b>	<b>35</b>
6.1 Conclusion . . . . .	35
6.2 Discussion . . . . .	35
<b>A Simulation Manual</b>	<b>37</b>
A.1 Overview . . . . .	37
A.2 Different Simulators . . . . .	37
A.3 Simulation results. . . . .	37
A.4 Addon datalink ADS . . . . .	40
<b>Bibliography</b>	<b>41</b>

# Chapter 1

## Introduction

### 1.1 Background on the ADome

Developments in wireless communication ever move towards higher frequency bands. Most recently, the first frequency range of the 5G standard for telecommunication is starting to become more adopted into mainstream consumer technology, with frequencies still below 6 GHz. The second frequency range foreseen for 5G, however, will range into the millimeter-wave spectrum.

Devices for the second frequency range of 5G-NR are currently being developed. With this move to higher frequencies substantially more bandwidth will become available, allowing for higher data throughput. However, higher frequencies also complicate the development of the communication systems. At these higher frequencies, to compensate for the increased free-space loss and increase directivity of the system, antennas are often combined into arrays to use beamforming. These arrays are frequently designed as a monolithic entity to enable further miniaturization. This makes individual testing of subsystems very complicated to impossible, increasing the relevance of over-the-air (OTA) testing.

In its current form, OTA characterization is a cumbersome process. The most used method involves near- or far-field scanning using a single probe that moves around the antenna-under-test (AUT). Another widely used technique is often known as a Compact Test Range (CATR), where a secondary feed antenna is used with a precisely manufactured reflector to create a region of plane waves where the AUT is placed. The AUT is then rotated in this field of plane waves to measure the response for different angles.

These methods both share weaknesses: they are relatively slow, due to only being able to measure a single point at a time. They require mechanical elements, increasing complexity and points of failure. Additionally, current testing methods typically use a network analyzer in their testing, requiring large lengths of RF cables to the AUT and probing elements.

To solve this problem, the ADome concept has been proposed. The ADome consists of detectors arranged in a half-sphere, each with its own antenna and RMS power detector, allowing the calculation of received power to take place at the node itself. It is a far-field measurement method, but the far-field distance at 5G mm-wave frequencies and above is sufficiently small that it comfortably fits into a regular laboratory. A picture of the structure of the current version can be seen in figure 1.1.

### 1.2 ADome Subprojects

A number of projects were carried out by this group to improve the current ADome prototype. These projects are mostly disconnected from each other as they all consider a different part of the system.

The first project is a new readout protocol. As the sensing probes acquire the measurements locally, the need of a readout protocol becomes necessary for the computer to process these data. The current implementation in the ADome is limited in its functionalities. Antenna probes locations must be computed manually, making it not user-friendly and difficult to use in case of large number of sensing antennas. Furthermore, the probes are not able to store any information, such as its own location.

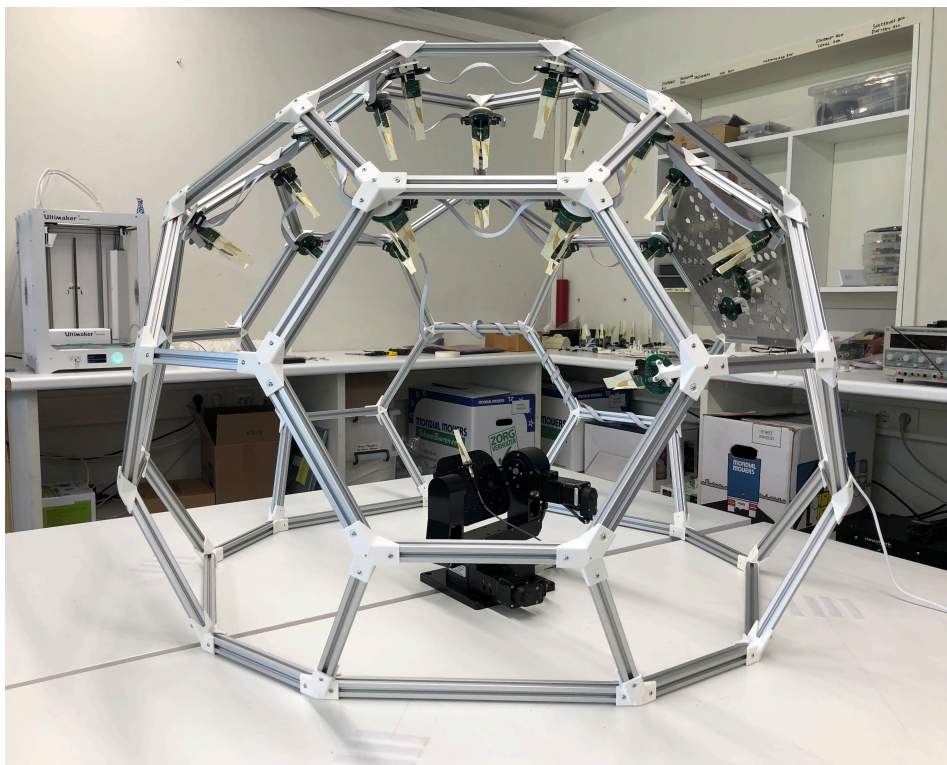


Figure 1.1: Structure of the ADome in development

Therefore, a new readout protocol using CAN is proposed where a micro-controller unit (MCU) is integrated at each probe to allow local sampling and readout along with non-volatile memory storage. Due to the presence of local MCUs, the potential functionalities of the ADome can be extended.

The second project concerns an optical calibration system. At the moment, the location of each sensor node needs to be measured and entered manually in the readout system. This project proposes a method to automatically determine the positions of the antennas in the dome. This is done using a camera mounted in the center of the ADome. The antennas will be recognized from the images taken by the camera using computer vision algorithms and the location in the images is mapped to a location in the dome.

This document details the third project, which is an uncertainty assessment of the sensing nodes. The ADome sensing nodes use a RMS power detector to measure the received power. This project aims to characterize the measurement uncertainty of the detector for different excitations. A simulation testbench of the measurement setups is also created to allow assessing the impact of changes in the system without needing to change the physical setup. Characterizations is done for single- and multi-tone signals at different frequency and power levels.

### 1.3 Problem Statement

As mentioned above, the main goal is the determination of the power detector response for varying setups. Part of this determination is done using measurements. Based on these measurements a simulation testbench is created that can be used to determine the response for setups that have not been physically measured.

The testing of the detector was limited to a frequency range of 20 GHz to 26 GHz. The 5G-mmwave spectrum starts at 24 GHz, but due to equipment limitations the frequency could not go above 26 GHz, so the range was extended downwards.

## 1.4 *State of the Art Analysis*

Antenna measurement using multiple probes simultaneously is not a concept unique to the ADome, as multiple other projects exist, for instance [5, 7, 13]. However, these are also in early stages of development and information about the probes used is scarce.

Power detectors are an important component of RF systems, so development of detectors for higher frequencies is an active field. This project focuses on the power detector used in the ADome, the LTC5596. This is a true-RMS or square-law detector. These devices typically use the I-V characteristics of semiconductor devices to convert the input signal into a DC level corresponding to the power level. [2]

The development of semiconductor-based devices for mm-wave can be detailed in [11, 15, 18], but these are mostly out of the range of interest for this project. A detector of similar range is described in [16], but it only states simulated results and little information about performance to different excitation modes. On the other hand, [19] details a RF power detector at a lower frequency range, that also shows a good response to modulated waveforms. In [6] discusses RF detector response to multi-tone signals, but as we will not have access to the internals of the chip, the bias voltage manipulation method is not that relevant. A two-tone response curve is also shown in [17], with fairly good correspondence to the single-tone curve.

## 1.5 Thesis Structure

This document is structured as follows. After this introduction, the programme of requirements of this project is presented in chapter 2. In chapter 3, an overview of the measurement setups and the equipment used in them is given, including a description of uncertainty sources. The simulation setup and results are shown in chapter 4. Finally, results from the measurement setups are presented in chapter 5. The thesis concludes with a conclusion and discussion section in chapter 6.



## Chapter 2

# Programme of Requirements

Based on the problem definition stated in the introduction, we can define a number of requirements that the measurement setup results need to meet.

The programme of requirements is split into the physical measurement setup and the simulation testbench, as the problem statement also consists of two parts.

### 2.1 Measurement Setup and Results

1. The measurement setup must deliver a characterization of the detector response under continuous wave excitation.
2. The measurement setup must deliver a characterization of the detector response under multi-tone excitation, for various amounts of tones.
3. Optionally, the measurement setup can deliver a characterization of the detector response for QAM-excitation.
4. The measurement setup must deliver a characterization of the detector response under over-the-air (OTA) continuous wave excitation.

### 2.2 Simulation

1. The simulation must be an accurate representation the measurement setups.
2. The simulation must contain the noise components of the power detector and the function generator.
3. The simulation must with the use of a Monte Carlo describe the expected accuracy of the detector, and give an error bound of the simulation with the measurements.



## Chapter 3

# Measurement Setups

In the following section the three setups used for measurements and recreated in simulations are discussed. The measurements are further discussed in chapter 5 and the simulations in chapter 4. In this an overview of the setups is given, and the equipment used is discussed.

### 3.1 Continuous Wave Direct Connection

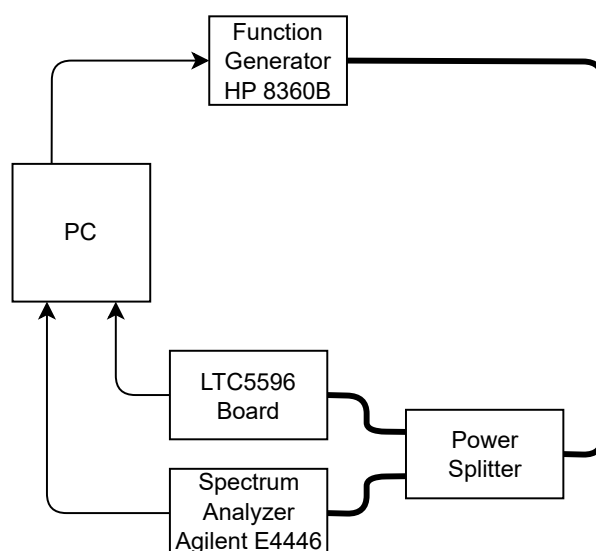


Figure 3.1: Schematic of measurement setup for continuous wave excitation

This is the simplest measurement setup, with only a single frequency signal and a direct connection between the signal and the power meter. A function generator is used to generate a single-tone waveform of varying power levels. To get a measurement of the power received at the detector, the signal is fed through a power splitter, where the power level is the same in both branches. One output of the power splitter is connected to the detector board, the other to a spectrum analyzer. All devices are connected to a computer used to control the equipment and save the results. A schematic overview of the connections can be seen in figure 3.1. In the following subsections the different equipment used are discussed.

#### 3.1.1 The Power Detector Board

The sensor nodes used in the current version of the ADome integrate the used antenna directly with the RMS detector and ADC on an PCB. This makes characterizing the performance of the system a more

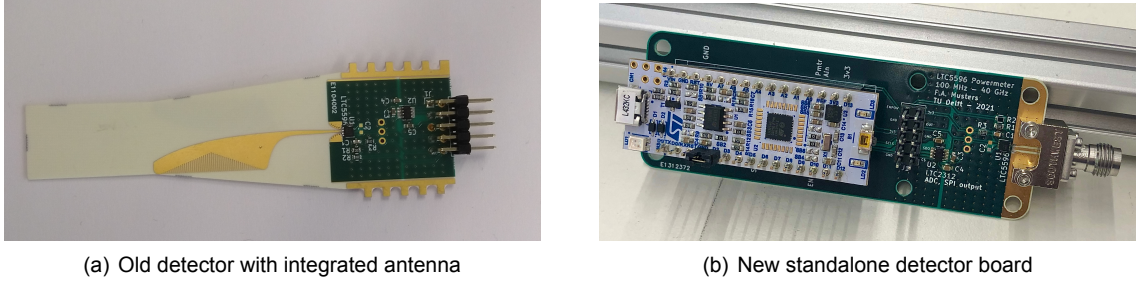


Figure 3.2: The old and new detector boards

difficult task, as it is not possible to directly compare the received power with another power meter. To do this the power received from the antenna need to be split between the antenna and the RMS detector.

To alleviate this issue, a standalone RMS power detector with a coaxial connector instead of the directly connected antenna was created as seen in figure 3.2. This board allows the connection of cables directly to the input of the RMS detector. The standalone circuit board also has an integrated micro-controller for readout of the ADC.

### The RMS Detector

The RMS detector used in the ADome is the Analog Devices LTC5596[10], a true-RMS detector that outputs a DC voltage that is linear in dB with the input power, therefore logarithmic with the input power. The accuracy of the power detector is mainly dependent on four variables.

Firstly the output noise of the detector is dependent on the noise generated by the chip itself. This is almost a flat noise floor over power and frequency. When the input power is 0 dBm the integrated output noise between 1 kHz and 6.5 kHz is  $22 \mu\text{V}_{\text{rms}}$ . To determine the noise power we need to know noise bandwidth. The sampling speed of the ADC is 500 kS/s, and according to Nyquist we then have a noise bandwidth of 250 kHz. Where after we can conclude that the output noise floor of the power detector is  $0.15 \text{ mV}_{\text{rms}}$ . However in practice this is more in the range of  $1.5 \text{ mV}_{\text{rms}}$ .

Secondly the input noise, this will be later discussed however in short. The power detector has an input noise that is dependent on the bandwidth of the chip, the bandwidth of the chip is 40 GHz however the power detector also integrates over time and therefore the noise bandwidth is smaller. The input noise influences more the lower power levels.

Thirdly the power detector has non-linearity, which means that the the linear in dB relationship between voltage and power is not perfectly linear. This depends on temperature but for temperatures around  $25^\circ$  the error is between 0 dB and 0.8 dB.

And lastly the matching creates a certain level of uncertainty. In figure 3.3 the insertion loss can be seen. Insertion loss will be later explained in section 3.1.3 but for now we can take the result which says that the error in the range of 20 GHz up to 26 GHz is 0.7 dBm.

All these errors will be taken as uncertainties. Then they are all placed together in table 3.1.

### The ADC

The readout board uses a Analog Devices LTC3212-12 ADC to convert the output voltage of the RMS detector into a signal to be processed by the computer. This ADC has a resolution of 12 bits and generates an internal reference voltage of 2.048 V, therefore the resolution of the ADC is  $\frac{2.048}{2^{12}} = 500 \square\text{V}$ .

For an ideal quantizer, the standard deviation, or RMS value, of the quantization noise can be calculated from the resolution according to equation 3.1, where  $q$  is the resolution. The quantization noise dominates for ADCs up to 16 bits[9]. Therefore this is a good approximation of the output noise.

$$\sqrt{e^2(t)} = \frac{q}{\sqrt{12}} = 4.1667e - 5 \quad (3.1)$$

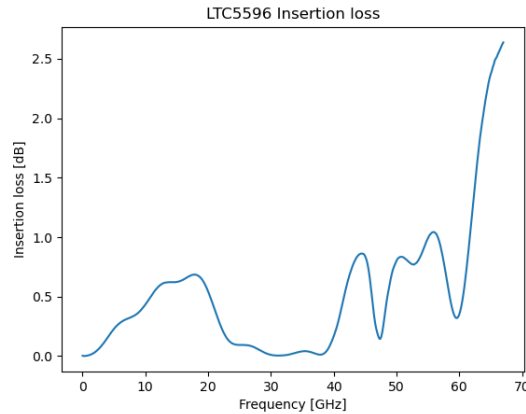


Figure 3.3: Insertion loss LTC5595

Table 3.1: The uncertainties for the antenna nodes.

Source of uncertainty	Symbol	Value	Probability distribution	Divisor
Noise generated	$V_f$	1500 $\mu$ V	Gaussian	1
Input noise	$V_f$	depends on $P_{in}$	Gaussian	1
Linearity error	$V_{In}$	0.8 dB	Gaussian	3
Matching error	$M_{pd}$	0.7 dB	Gaussian	3
ADC quantization noise	$N_Q$	250 $\mu$ V	Rectangular	$\sqrt{3}$

### 3.1.2 Function Generator

The function generator 8360B from Keysight generates one frequency with a certain power level. The generator will do a frequency and a power sweep. Therefore the uncertainty of them both needs to be taken into account. According to the datasheet there is an accuracy and flatness specification. The accuracy usually describes the absolute power deviation for any frequency. The flatness specification is lower than the accuracy specification and it is usually referenced to the amplitude of the first frequency before the frequency sweep[3]. For our purpose the accuracy specification is more accurate. The numbers in the datasheet are for an uncalibrated system. Therefore testing is needed to know to what extent the function generator is calibrated. However after testing we came to the conclusion that the values given in the datasheet are quite accurate.

Source of uncertainty	Symbol	Value	Probability distribution	Divisor
Accuracy	$P_{gen}$	1.2 dB	Gaussian	2

Table 3.2: The uncertainties of the function generator

### 3.1.3 Spectrum Analyzer

The spectrum analyzer is used to know the power of the signal sent, and used to measure the noise floor later on. The spectrum analyzer has a relative and an absolute uncertainty. Relative uncertainty is the uncertainty in the difference in amplitude between two peaks. Absolute uncertainty is the uncertainty in amplitude and therefore measured input power of the signal. Absolute power is the thing we are interested in and the absolute uncertainty will therefore be considered. In the following subsections the different uncertainty components are explained.

### Flatness

The input attenuators and mixers create amplitude changes with frequency. This is what makes the frequency response less flat. With flat we mean no changes of the response over frequency. The response is made more flat with the use of a calibration method. This is done with the use of a calibrator signal of 50 MHz.

### Reference level accuracy

The reference level is traditionally defined by the amplitude represented at the top line of the graticule on the display. The amplitude of this line is dependent on the reference level, the attenuation and the IF gain. The reference level is calibrated with a known signal. The uncertainty of this calibration sets the reference level accuracy. The attenuation level changes also the calibration uncertainty due to another calibration signal is needed.

### Log-linearity fidelity uncertainty

The spectrum analyzers power is shown in logarithmic scale and therefore traditionally a log amplifier is used which has a linearity error can cause uncertainty in the power measurement. This is called the log-linearity fidelity uncertainty. Even though the current spectrum analyzers don't have the amplifier this error will nevertheless be present. This error is due to RF compression below -20 dB and ADC range gain alignment limitations.

### Dithering

Like described in the section of the ADC the ADC can have a quantization error. For low power this can be really significant. The ADC will also have linearity errors, however when there is noise added at the input which is larger than the most significant bit the linearity error can be really small due to the smoothing of the noise. This added noise is called dither and because it is added on the complete frequency range this cannot be seen on the display. When off the noise level is lower but the linearity error is smaller.

### Internal calibration

The internal calibration is dependent on the calibration signal. However if the calibration signal is the same for the power generator this error does not need to be taken into account. Because the generator and the function generator have this error this doesn't need to be taken into account.

### Matching uncertainty and error

Not all the energy that is incident on the spectrum analyzer is received by the spectrum analyzer. This loss is taken into account with the characterization of the complete chain however when the spectrum analyzer is compared with the power detector this error will come up. The matching loss is calculated with equation 3.2. The uncertainty of this error is given by equation 3.4.

$$\text{mismatch loss} = 20\log|1 - \Gamma_{\text{spectrum}}\Gamma_{\text{cable}}| - 10\log(1 - |\Gamma_{\text{spectrum}}|^2) \quad (3.2)$$

Where  $\Gamma_{\text{spectrum}}$  is the reflection coefficient of the spectrum analyzer and  $\Gamma_{\text{cable}}$  is the reflection coefficient of the cable. The VSWR of the cable is around 1.2 and the VSWR of the spectrum analyzer is between 1 and 1.4. The VSWR can be easily converted into reflection coefficient with the use of equation 3.3. When all the values are filled in for equation 3.2 we can conclude that the mismatch loss is 0 dB and 0.1 dB.

$$\Gamma = \left| \frac{VSWR - 1}{VSWR + 1} \right| \quad (3.3)$$

However we also don't know the phase of both the reflection coefficients. The maximum and minimum error of the consequence of that can be seen in equation 3.4. From that we can calculate that the matching uncertainty is  $\pm 0.13$  dB.

$$\begin{aligned} M_{uMax} &= 20 \cdot \log(1 + \Gamma_{\text{spectrum analyzer}} \Gamma_{\text{cable}}) \\ M_{uMin} &= 20 \cdot \log(1 - \Gamma_{\text{spectrum analyzer}} \Gamma_{\text{cable}}) \end{aligned} \quad (3.4)$$

## Conclusion

The calibrator error, log-linear fidelity uncertainty, IF gain uncertainty, and RBW switching error are all combined under the name absolute amplitude uncertainty. Therefore the resulting uncertainties are the reference level uncertainty and the absolute amplitude uncertainty. Which is a combination of the frequency response and the absolute amplitude response.

Symbol	Source of uncertainty	Value	Probability distribution	Divisor
Reference level	$R_L$	0.05 dB	Gaussian	2
Absolute amplitude response*	A	0.06 dB	Gaussian	2
Frequency response	$F_r$	1.3 dB	Gaussian	2
Matching phase uncertainty	$M_{\text{phase}}$	0.13 dB	Gaussian	2
Matching loss uncertainty	$M_L$	0.1 dB	Gaussian	2

Table 3.3: Uncertainty of the spectrum analyzer. \* linearity, RBW, switching, attenuator, Freq. tuned to the input CW freq

### 3.1.4 The Cables

The cables will be characterized and therefore shouldn't bring addition uncertainties. However due to the way the characterization is averaged over different power levels an error for both the spectrum analyzer and the power detector arises this error is approximately  $\pm 0.3$  dB. However from the splitter there are two cables. One towards the function generator and one towards the power detector. When the matching with the splitter is unequal they create an error and therefore an uncertainty. It is hard to define this error but nevertheless. An approximation of  $\pm 0.2$  dB has been chosen.

### 3.1.5 The Power Divider

The power dividers also called wilkinson power dividers are passive devices that split the power into two parts. The datasheet for this particular device has not been found but similar devices have an balance uncertainty of around  $\pm 0.2$  dB.

Symbol	Source of uncertainty	Value	Probability distribution	Divisor
Balance uncertainty	$R_L$	0.2 dB	Gaussian	2
Cable characterization	C	0.5 dB	Gaussian	2

Table 3.4: Uncertainty of power splitter

## 3.2 Continuous Wave Direct Connection OTA

In this measurement setup an over-the-air connection is added to the signal path. This is done get a better understand in how the system behaves in an over the air measurement. The signal still consists of a single-tone signal. To compensate for the additional losses added by the antennas and the free-space propagation, an amplifier is added before the transmit antenna. The antennas used are of the same type as used in the sensing nodes of the ADome and are aligned in the same plane. A schematic of this setup is depicted in figure 3.4

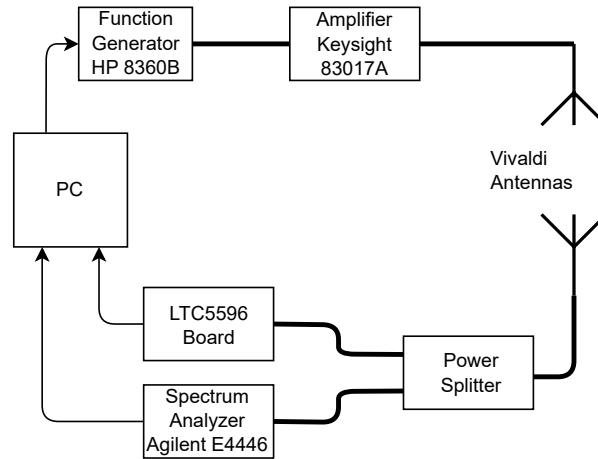


Figure 3.4: Schematic of measurement setup for continuous wave OTA excitation

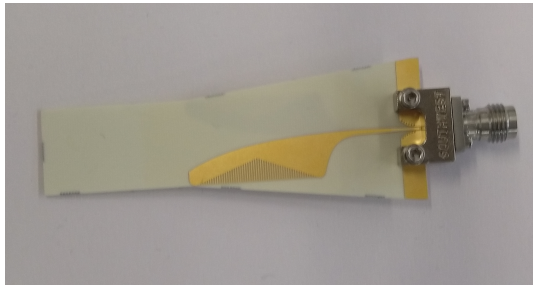


Figure 3.5: Vivaldi antenna used in the OTA setup

### 3.2.1 Amplifier

The amplifier has as purpose to amplify the signal to reach the complete dynamic range of the power detector. However the amplifier doesn't have a flat power response. It therefore has a big uncertainty of  $\pm 1.1$  dB. However the amplifier together with the cables has been characterized and therefore this uncertainty has not been taken into account. The model of amplifier used is a 83017A.

### 3.2.2 The antenna and free space loss

The antenna described in [12] is used in this setup. It are two antennas directly connected to a coax cable. They are placed opposite of each other. The antenna is a single Vivaldi antenna connected to the board. The antenna gain is earlier measured[12] and can be seen in figure 4.11. The uncertainty of the antenna alignment is depended on multiple things but mainly three. There could be a bigger space between the antenna then measured. Secondly due to polarization of EM waves part of the energy could not be received by the antenna. Thirdly the antennas have passive gain in one direction, and if they are not properly aligned part of this gain is lost. All these effects cannot be easily quantified therefore it is chosen to give an estimate with the use of free space loss. The equation of free space loss is equation 3.5. where  $d$  is the distance in meters and  $c$  is the speed of light. This will later be further discussed but for now we conclude that an uncertainty of alignment of 5 mm is around 0.4 dB.

$$\text{FSPL} = 20 \cdot \log\left(\frac{4\pi df}{c}\right) \quad (3.5)$$

Symbol	Source of uncertainty	Value	Probability distribution	Divisor
Antenna and LOS uncertainty	L	0.4 dB	Gaussian	2

Table 3.5: Uncertainty of free space loss and antenna gain

### 3.3 Multi-tone Direct Connection

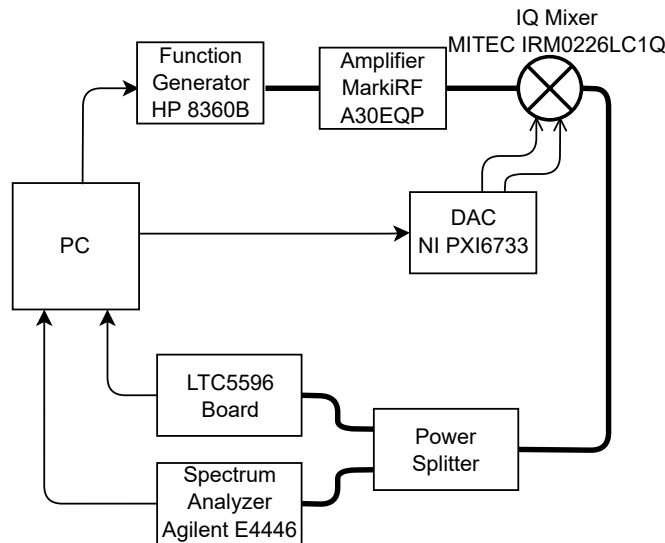


Figure 3.6: Schematic of measurement setup for multi-tone excitation

With this configuration the response of the LTC5596 board to a multi-tone excitation is benchmarked. To generate the multi-tone signal, an IQ mixer is used. To ensure the mixer receives sufficient input power a small amplifier needs to be inserted before the mixer. The modulation waveforms for the mixer are provided by a DAC. The output of the mixer is connected directly to the power splitter. Because the input power to the mixer must stay inside a small range to operate, changing the power of the signal must be done in a different way. The power of the output waveform is instead changed by changing the amplitude of the I and Q modulating waveforms.

An additional step must also be introduced when calculating the received power on the spectrum analyzer, as a single peak measurement is not enough to get the total received power. Instead, the power in all the peaks must be summed. This is done after the measurement, so from the spectrum analyzer the trace is exported and later processed.

#### 3.3.1 IQ Mixer

The IQ mixer model is a MITEC IRM0226LC1Q. To operate reliably, the mixer needs a input power between 10 dBm to 12 dBm. With cable losses, this is slightly above the maximum output power of the function generator, so an additional amplifier is needed.

The mixer also suffers from some non-ideal behavior. Firstly, at zero voltage applied on the I and Q inputs, some of the continuous wave is still transmitted to the output. By applying the correct bias voltages on the inputs, this can be compensated for and the carrier feedthrough can be reduced. Secondly, the difference between the in-phase and quadrature waveforms is not quite 90°, and they do not have the exact same amplitude. These errors is not relevant for this application, as the phase does not play a role in the creation of the multi-tone waveform. This phase and amplitude error is thus not compensated in the current system. To reduce the carrier feedthrough, the bias voltages have been determined beforehand per frequency and are applied as DC offset to the I and Q waveform.

#### 3.3.2 The Pre-Mixer Amplifier

The amplifier used is a Marki RF A30EQP, providing approximately 10 dBm of gain, which reduces with frequency, meaning that different powers need to be set at the function generator for each frequency to ensure a similar output power.

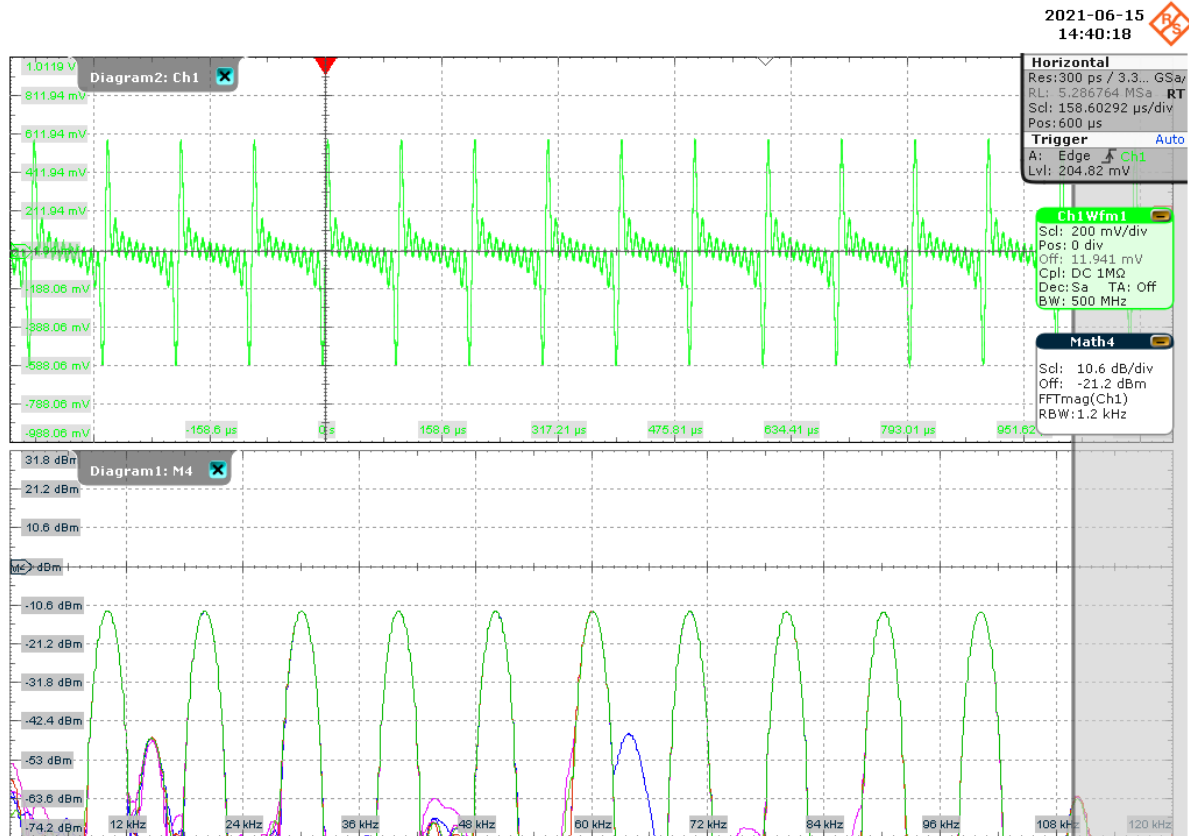


Figure 3.7: Oscilloscope Trace for a 10-tone waveform

### 3.3.3 The DAC

The DAC used is a NI PXI6733. This model has a maximum sample rate of 1 MS/s. With the DAC included was a scaling buffer module, scaling the voltage output down from a range of  $-10\text{ V}$  to  $10\text{ V}$  to a range of  $-0.8\text{ V}$  to  $0.8\text{ V}$ , allowing the use of the full DAC resolution over a smaller voltage range. However, the DAC does not have an output buffer, so depending on the frequency requested a significant number of harmonics may be introduced.

A minimum of 10 samples for a sine wave was chosen, limiting the maximum frequency that can be created to 100 kHz. The signals generated have evenly spaced tones, so the minimum frequency is determined by  $\frac{f_{max}}{n_{tones}}$ . This minimum frequency in turn determines the length of the waveforms to be transmitted to the DAC, as a lower frequency will require more samples for a full period. Using evenly spaced tones, the frequencies are all multiples of each other, so an integer number of periods fits into the number of samples needed for the minimum frequency. The waveforms generated were first verified using an oscilloscope, an example of which can be seen in figure 3.7, showing a waveform with 10 tones.

## 3.4 Software Setup

The equipment needed to be controlled in different ways. The function generator and spectrum analyzer could be controlled using the GPIB bus, using the VISA standard. The detector readout board has a microcontroller that receives its command via a serial port, and the DAC connects to the computer using a PCI-Express cable and requires the use of National Instruments tools to be controlled. To unify all this, the Python programming language was used to write some scripts combining the functionality, as libraries were available for all these communication types:

1. For GPIB over VISA the `pyVISA` package was used, with the Keysight-VISA backend.
2. For serial communication, the `pySerial` package was available
3. For communication with their devices, National Instruments have create the package `nidaqmx`, which creates bindings to the NI DAQ API.



# Chapter 4

## Simulation

In this chapter the simulations made in ADS of the previous setups are discussed. For all the equipment it is explained how it is modeled. A noise simulation and a Monte Carlo simulation is made to combine the uncertainties as discussed in the previous chapter. The manual for the simulation can be found in appendix A.

### 4.1 Continuous Wave Direct Connection Setup

The direct connection setup, as discussed earlier in figure 3.1. Is simulated with the use of ADS and shown in figure 4.1. The setup contains a function generator, whereafter a cable is connected which is implemented as an s-parameter block. After which a power splitter is added. At one end the power detector is added and at the other end a spectrum analyzer is connected.

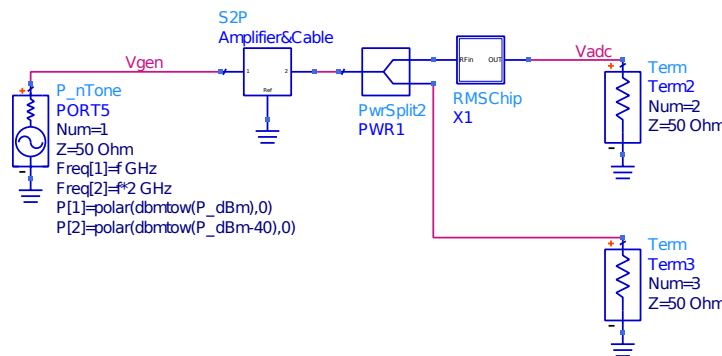


Figure 4.1: Direct connection setup

The simulation uses a harmonic balance simulation. This simulation type only simulates the system in frequency domain, where it only looks at certain tones and orders of that frequency. Therefore it is fast and descriptive. But it does not describe other frequencies as well as transient.

#### 4.1.1 Equipment

##### The function generator

The function generator is modeled with the use of a component called a tone generator. There are two tones generated: the main frequency and its harmonic. The harmonic is 40 dB lower according to measurements. Sub harmonics have been modeled, but we later removed because they had an insignificant effect. Phase noise is also added and will be discussed in section noise simulation.

## The Power Detector

The power detector is modeled in ADS and made a separate component with a separate schematic. The model can be seen in figure 4.2. There are multiple ways to model the power detector, a choice

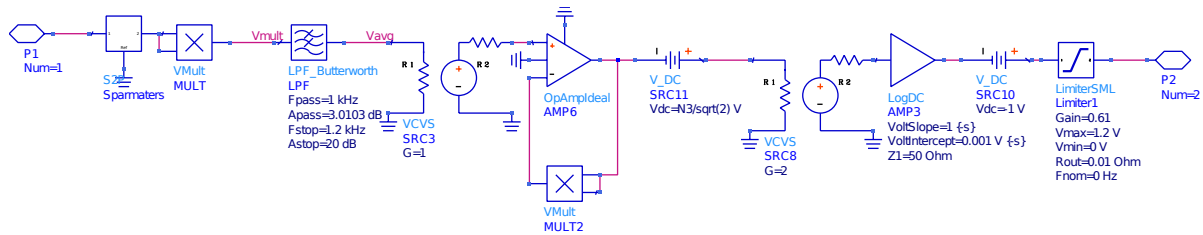


Figure 4.2: RMS power detector schematic

is made to model it as the mathematical representation because of its simplicity to understand and modify for different power meters. The chip represents the root-mean-square function (RMS). The RMS function is defined in equation 4.1.

$$f_{\text{RMS}} = \sqrt{\frac{1}{T_2 - T_1} \int_{T_1}^{T_2} [f(t)]^2 dt} \quad (4.1)$$

First, the square is taken with the use of the multiplier component. After this the mean is taken. An equivalent model of the mean is a low-pass filter. The simulation works in the frequency domain and therefore a low-pass filter needs to be used. Therefore a low-pass filter is implemented, with a steep roll-off after 1 kHz. The exact cutoff point doesn't matter because the simulation simulates in orders of 100 kHz. Lastly, the square root is modeled with a multiplier in the feedback loop of an perfect amplifier.

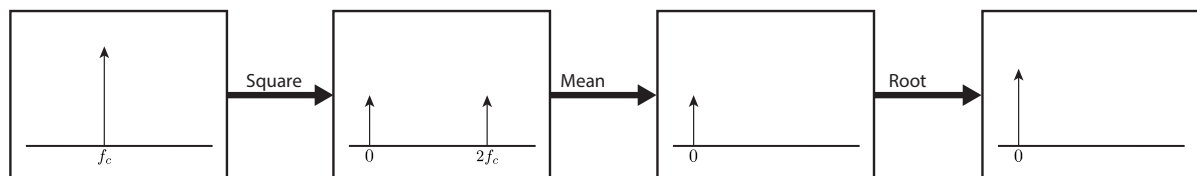


Figure 4.3: Taking the root-mean-square

The power detector voltage output has a logarithmic response to the input power. Therefore, a logarithmic amplifier is used. The height of the response curve is determined with a DC voltage source. The slope of the response curve is determined with the gain of a limiter component. These two parameters are selected such that the simulation slope is aligned with the measurement slope. In figure 4.4 the response is shown to be versus frequency. The frequency response of the power detector mainly depends on two factors: the s-parameters (insertion loss) and the linearity error. The linearity error has been added as an uncertainty and the insertion loss has been added as an s-parameter. The input s-parameters were downloaded from the supplier and the insertion loss can be seen in figure 3.3. While the s-parameters is not an uncertainty in the setup, it will probably be an uncertainty in the final use.

The last step is the maximum voltage and therefore the dynamic range of the power detector. This is modeled with a voltage limiting component. It has a range of 0 V up to 1.2 V.

## Cables

It is possible to model the cables and their connectors in at least two ways. One is to model the expected physical behaviour of the cables and their connectors. The other way is to characterize the chain of cables and to determine the losses in this way. The second option has been chosen because it is more accurate and a lot of uncertainties do not need to be taken into account. The power loss is measured with the spectrum analyzer. The resulting loss is put into a s-parameter block as to describe an perfect amplifier. However the gain seems to be dependent on power. This is most likely due to the function

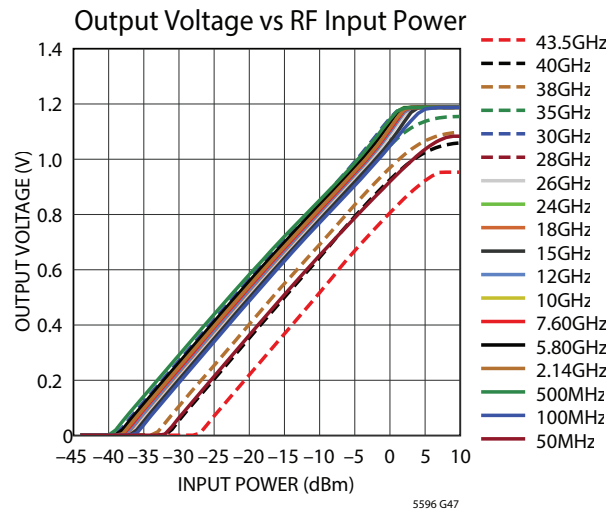


Figure 4.4: Output voltage versus input power according to the datasheet

generator itself having an offset. It still creates some error, for both the spectrum analyzer and the power detector in the simulation. Which can be approximated with a  $2\sigma$  of  $\pm 0.3$  dB.

### 4.1.2 Noise Simulation

The noise simulation describes the different noise components of the system. This part will be divided in the noise of the detector and the noise of the system behind the detector. It has been chosen to limit this simulation due to difficulties with the simulation, therefore the phase noise and the noise floor at the input of both detectors are discussed and their impact on the output of the detector. How the noise behaves through the full chain of cables and amplifiers will not be discussed.

#### Phase Noise

Phase noise is noise in the phase of the signal. The phase noise can also be seen as deviations in the frequency domain from the carrier frequency. It can be explained as follows. White noise is random and contains many frequencies. All these frequency components have a phase with respect to the carrier frequency, which is also random. However, when we look at the addition of a noise voltage with a sinusoidal voltage we get figure 4.5. We can therefore see that a noise in phase makes a deviation of the carrier frequency between a certain frequency band. The result can be seen as a smear over this frequency.

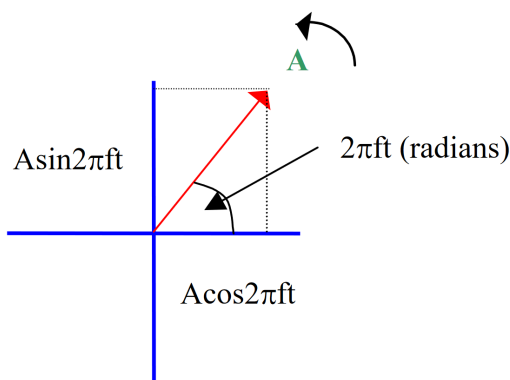


Figure 4.5: The addition of the phase noise vector with the signal [1]

In practice, phase noise is added in the function generator and the spectrum analyzer. The phase

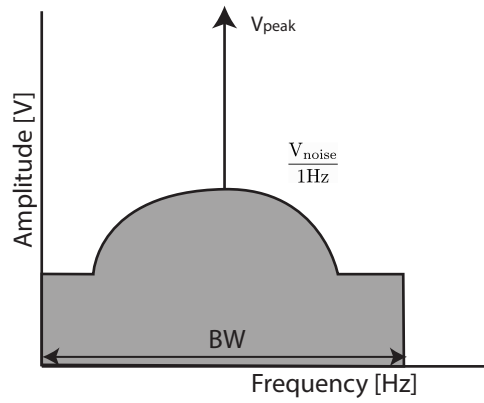


Figure 4.6: The noise voltage of a 1 Hz noise bandwidth

noise of the function generator is simulated in ADS with the use of an option inside the tone generator component. The phase noise of the spectrum analyzer has not been implemented, because there was no option found to do it. The phase noise of the spectrum analyzer consists of two effects: the windowing phase noise and the added phase noise due to the internal hardware of the spectrum analyzer. The windowing phase is caused by a window that is thrown over the signal, this is caused by the integration over the resolution bandwidth. The phase noise is measured with the spectrum analyzer.

### The Noise Floor Measurements

The noise is measured using the spectrum analyzer with a span of 1 GHz. First, the noise level is measured with an averaging factor of 128. Next, the RBW, reference level and attenuation are subtracted. Which results in the power in bandwidth of 1 Hz. The noise bandwidth of the simulation is also 1 Hz. This improves the consistency within the simulation.

$$P_{\text{noise}} = P_{\text{noise level spect.}} - 10 \log_{10} \left( \frac{\text{RBW}}{1\text{Hz}} \right) - \text{Reference level (dB)} - \text{Attenuation (dB)} \quad (4.2)$$

### SNR, THD and SINAD

To know the quality of the signals that are measured by the power detector, we can look at the signal to noise ratio (SNR), the total harmonic distortion (THD) and the combination of signal to noise and distortion ratio (SINAD). This is all done within ADS.

The signal to noise ratio is defined as the ratio of the signal power to the noise power.[8] In decibels the equation results in equation 4.3.

$$\text{SNR} = 10 \log_{10} \left( \frac{S}{N} \right) \quad (4.3)$$

When both S and N are measured over the same impedance, we can say that  $\frac{S}{N} = \frac{A_{\text{signal}}^2}{A_{\text{noise}}^2}$ . Thereby, we can calculate the noise power N by integrating the squared noise voltage density of a 1 Hz noise bandwidth, as seen in figure 4.6 over a bandwidth.

$$N = \int_{f_c - BW/2}^{f_c + BW/2} V_{\text{noise}}^2(f) df \quad (4.4)$$

We can say that the signal is the sum of the squared carrier frequencies:

$$S = \sum_{n=1}^N V_n^2 \quad (4.5)$$

However the noise is not the only unwanted signal in the frequency spectrum, so are harmonic and sub harmonic frequencies. The harmonic signals are multiples of the carrier frequency. The sub harmonics are on the  $1/n$  times the carrier frequency. The total harmonic distortion can be defined in two ways. But here we define it as follows: the ratio of the fundamental signal's RMS value divided by the harmonic's RMS value as shown in equation 4.6.

$$\text{THD} = 20\log_{10}\left(\frac{S}{D}\right) \quad (4.6)$$

Where the distortion is defined in equation 4.7.

$$D = \sum_{n=1}^N V_{\text{harmonic order } n}^2 \quad (4.7)$$

The combination of the harmonics and the noise describe the quality of the signal.

$$\text{SINAD} = -10\log_{10}\left(10^{-\text{SNR}/10} + 10^{-\text{THD}/10}\right) \quad (4.8)$$

### Noise Simulation Results

**Noise at the input of the detector** The noise at the input of the power detector is dependent on two sources: the noise floor and the phase noise. Both of these sources are measured with the spectrum analyzer. The measured phase noise was  $-55$  dBm/Hz. When accounting for the noise figure of  $13$  dBm of the spectrum analyzer, this would result in a phase noise of  $-68$  dBm/Hz. The noise floor measured is  $-146$  dBm/Hz. The resulting noise floor would then be  $-159$  dBm/Hz at the input of the spectrum analyzer. This results in figure appendix A. Lastly, the SNR, THD and SINAD are calculated. The SNR is  $150$  dB, the THD is  $41$  dB, and the SINAD is  $41$  dB as well. Thus we conclude that the phase noise dominates the signal to noise ratio and therefore the input noise of the power detector. The harmonics are the main source of degraded signal quality.

**Noise at the Output of the Detector** There are three main contributors to the noise at the output of the chip. These contributors cause variation of the output voltage in time. The first source is the noise at the input of the power detector. Secondly the noise generated by the power detector itself. And lastly the noise added by the ADC. The noise bandwidth of the power detector is unknown, and therefore the noise it represents at the output is unknown. However, we measured the noise at the output and therefore the measurements and the simulations can be aligned. The noise generated by the power detector is also largely unknown. The noise source generated by the power detector and the noise source received are aligned with the measurements.

In figure 4.7 the standard deviation of the voltage is plotted versus the input power. This is done for both the simulation and the measurements. For the simulation a Monte Carlo simulation is used. Further information can be found in section 4.1.3. Next, the noise generated by the power detector and the noise at the input of the power detector are tuned, so that they align with the measurements.

In the end the RMS noise voltage of the input of the power detector was  $750 \mu\text{V}_{\text{RMS}}$ . The noise generated by the power detector itself was  $1.5 \text{mV}_{\text{RMS}}$ . We can see that the simulation alignes well with the measurements.

### 4.1.3 Comparison Power Detector and Spectrum Analyzer with Monte Carlo

Not all differences in power measured between the spectrum analyzer and the power detector can be modeled perfectly. They can, however, be described by uncertainties. Uncertainties were previously described for individual components of the setup. Now, these uncertainties will be combined with a Monte Carlo simulation, with which we find uncertainty bounds.

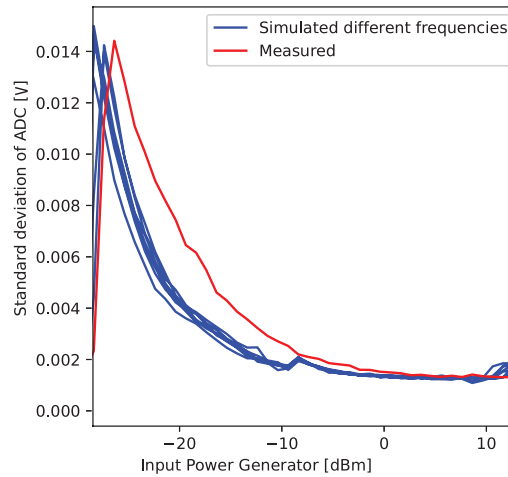


Figure 4.7: Standard deviation of the voltage at the output of the detector

### The Monte Carlo Simulation

The Monte Carlo simulation makes use of repeated random sampling to obtain numerical results. In the simulation, different components have variables with a Gaussian or Uniform distribution. Each iteration a change of a component depending on the distribution of a value of a component is made. After many iterations, a Gaussian distribution can be found. The number of iterations that are needed depends on the accuracy required and the expected standard deviation [4]. The standard deviation of the boundary decreases with the square root of the number of iterations. In figure 4.8 the standard deviation can be seen. We can conclude that after 1000 iterations the calculated standard deviation is around 95% accurate. Therefore it has been chosen to use 1000 iterations for all the Monte Carlo simulations.

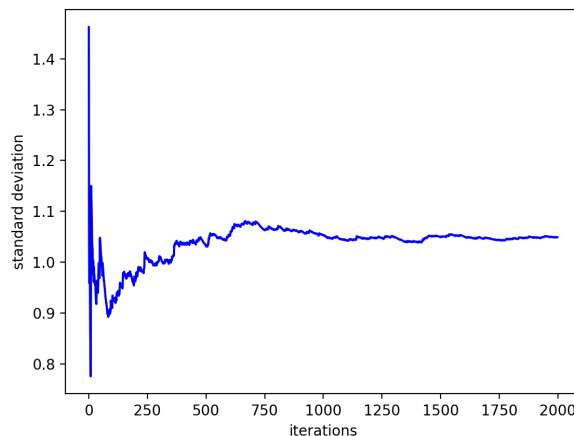


Figure 4.8: How the standard deviation changes over the number of iterations

The noise voltages are added with dc voltage sources. Power uncertainties are implemented with an amplifier. Further explanation can be found in appendix A. With the use of schematic A.4 a Monte Carlo simulation is simulated. The  $1\sigma$  accuracy bound can be acquired of the result. The power is swept and for each different input power a separate Monte Carlo simulation is run. Therefore, we can conclude that the measurements lie closely within the uncertainty bounds of three standard deviations.

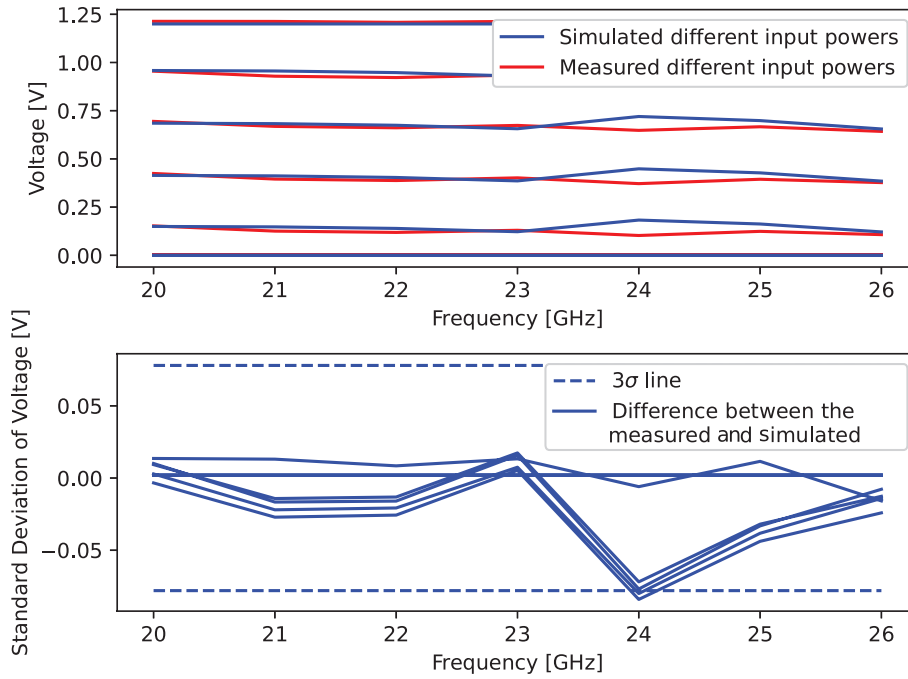


Figure 4.9: Uncertainty bound for direct connection setup

## 4.2 Continuous Wave Over-th-Air Setup

The continuous wave OTA setup as earlier discussed 3.4 is a modification of the previous setup. It adds an amplifier to amplify the signal whereafter it is transmitted and received by two antennas. This power that is received is again split and received by the spectrum analyzer and the power detector. The resulting schematic can be seen in in figure 4.10. Most analysis is already done at the previous setup and will not be discussed again.

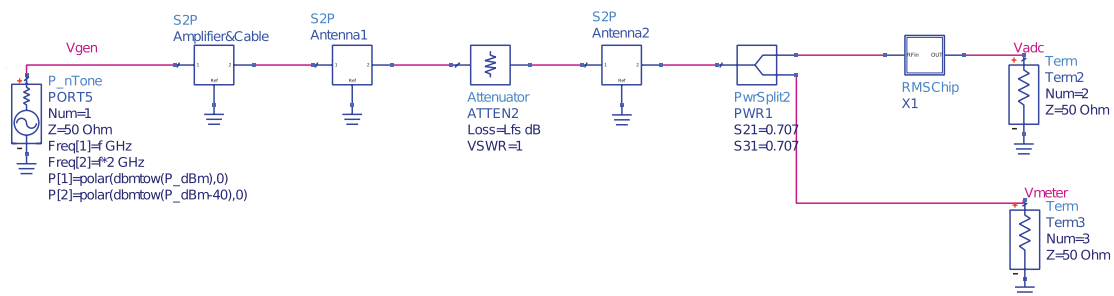


Figure 4.10: Schematic of OTA simulation setup

## 4.2.1 Equipment

### The Amplifier and Cables

To model the amplifier and cables the choice has been made to first characterize the complete chain with the use of the spectrum analyzer and then implement this as a gain in an s-parameter block. This gain is then dependent on frequency but not on power even though it is dependent on power. This because the amplifier is dependent on input power. Therefore this is an approximation and will not perfectly describe the actual power and frequency response. However this can mostly be seen at the higher power levels. This uncertainty however, can be quite significant. With the use of this characterization most of the matching uncertainty does not need to be taken into account. Another thing to note is that in this setup the setup has been rebuild after the characterization of the amplifier cable chain. Therefore a bigger discrepancy can be found between the measurements and the simulation. This will be approximated by  $\pm 0.5$  dB based upon measurements of the spectrum analyzer.

### The Antenna

The antenna described in [12] is used in this setup. There are two antennas connected to a coax cable a receiving and sending one. The gain of the antenna can be seen in figure 4.11.

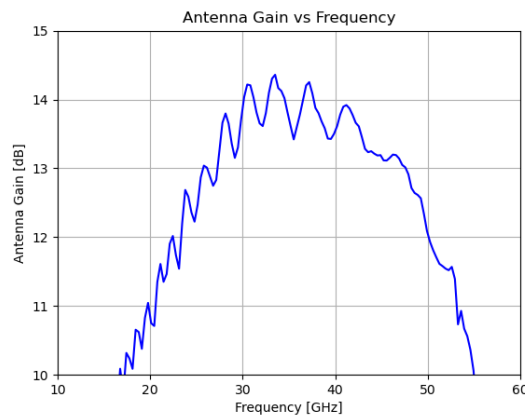


Figure 4.11: The antenna gain from [12, p.40]

An uncertainty of this configuration is the insertion loss. But the antenna gain has been measured, since the antenna gain contains the insertion loss the matching uncertainty is not being taken into account. The gain of the antenna is inserted with the use of a s-parameter component. The resulting s-parameter block describes a perfect amplifier s-parameter block. More information of s-parameters can be found in [14].

### Free Space Loss

The free space loss is modeled with the use of Friis equation 3.5. The attenuator component in ADS has been used to model the losses. The distance parameter is used to align the losses of the simulation with the losses of the measurements.

## 4.2.2 Noise Simulation Results

### Noise at the $RF_{in}$ of the detector

Due to time limitations and a change of setup later on in the process this has not been measured. Therefore no conclusion will be made.

### Noise at the Output of the Detector

To determine the noise at the output of the detector the same procedure as for the direct setup is followed. In figure 4.12 the standard deviation of the voltage is plotted and the simulation is aligned with the measurements.

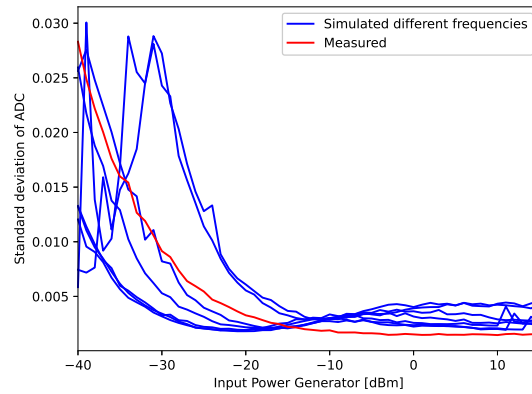


Figure 4.12: Standard deviation of the voltage at the output of the detector

In the end the rms noise voltage of the input of the power detector was  $1.05 \text{ mV}_{\text{RMS}}$ . And the noise voltage of the power detector itself was  $1.5 \text{ mV}_{\text{RMS}}$ . There can be noticed that the input noise is bigger but the noise generated from the power detector is the same. This makes sense because there is noise added due to the OTA setup and the power amplifier.

### 4.2.3 Simulation Check with Measurements

In figure 4.13 the uncertainty bounds can be seen. Due to the added uncertainty of the complete chain for both the function generator and the power detector the uncertainty boundaries are quit a bit larger. However the resulting measurements lay well inside the  $3\sigma$  boundaries.

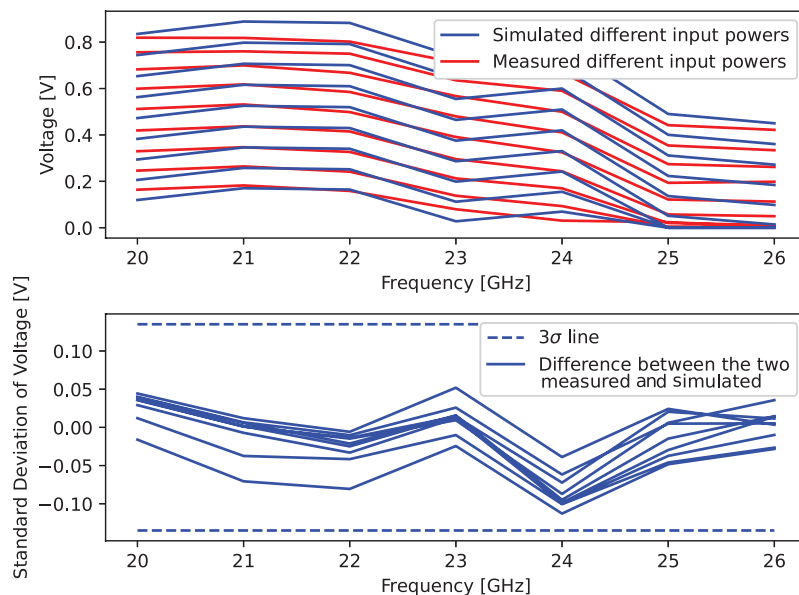


Figure 4.13: Caption

### 4.3 Multi-tone Direct Connection

The multi-tone setup is the same as the direct setup however the function generator has been replaced by a IQ mixer and a function generator and two other signal generators are connected. The schematic can be seen in figure 4.14.

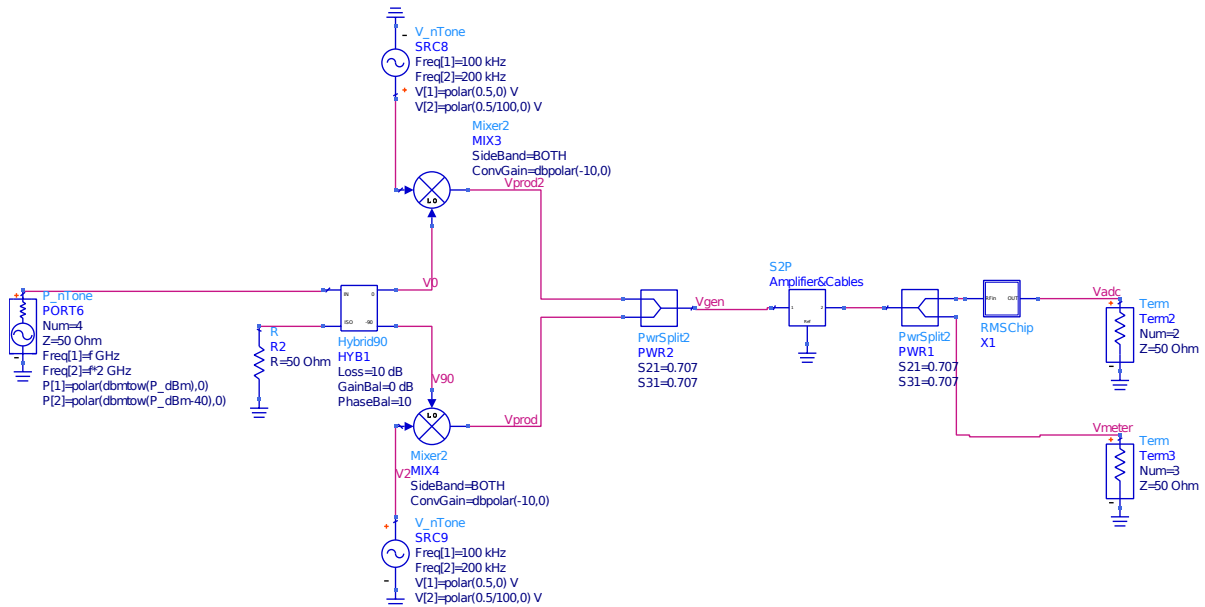


Figure 4.14: Multi-tone basic schematic

#### 4.3.1 Equipment

##### IQ Mixer

The IQ mixer is simulated using two separate mixer components. The LO leakage is built into the ADS mixer component, by changing a parameter the leakage can be adjusted. This parameter was set to  $-60$  dBm, which is the minimum achieved in the measurement setup. As phase and gain imbalance are not relevant for the multi-tone generation, these parameters were left unset.

##### DAC

The DAC is modeled as a multiple tone voltage source generator. The multiple tones describe the multiple tones from the DAC. One sub harmonic has been added for each tone.

#### 4.3.2 Noise Simulation

##### Noise at the input of the detector

The noise floor is the same as the previous setup after measurements. However, this time there are two peaks instead of one. The noise floor measured is  $-146$  dBm/Hz the resulting noise floor would then be  $-159$  dBm/Hz. Whereafter the SNR, THD and SINAD are calculated. The SNR is 150 dB, the THD is 41 dB, and the SINAD also is 41.4 dB Therefore we conclude that the phase noise dominates the signal to noise ratio and therefore the input noise of the power detector. And the harmonics are the main source of deviation from the input power.

**Noise at the Output of the Detector**

The noise at the output of the detector is suspected to be the same as before. Because the noise level and the phase noise is the same as before. However the harmonics have more influence on the signal as before.

**4.3.3 Uncertainty Bound Results**

The uncertainty bound is the same as for the direct connection setup. However this setup is too slow for a proper Monte Carlo analysis therefore it is advised to generate multiple tones with a tone generator or use a stored dataset.



# Chapter 5

## Measurement Results

These measurements were done using the setups that have been described before in chapter 3. To estimate the deviation of the power detector output voltage, 2500 samples were taken from the board for every measurement taken. To get a stable measurement from the spectrum analyzer, the averaging functionality was used with 128 averages.

### 5.1 Direct Connection

The measurement setup used for this part can be seen in figure 3.1. From the samples taken by the detector the mean and standard deviation is taken. Both of these are plotted against the power received by the spectrum analyzer. These plots can be seen in figure 5.1. The plot of the standard deviation starts at slightly higher powers than the mean, because at lower powers the measurements start to clip to 0 V, so the standard deviation calculated will be meaningless.

It is clear that the mean of the samples is linear with the received power, which is expected. The dynamic range of the detector is approximately 35 dBm. What is notable is that the curves for different frequencies are offset from each other. The offsets can be seen in figure 5.2, together with the slopes of the curves. While there are some variations in the offsets, and one large deviation, it is still possible to see that the maximum offset is 0.06 V, between the curves at 20 GHz and 26 GHz. The slopes are all approximately equal in magnitude, 0.03 V/dBm. Using the slope we can translate the offset in voltage to a power level. The maximum offset of 0.06 V then equals a maximum power offset of 2 dBm. In the slopes there is a large spike downward at about  $-25$  dBm, this is due to the fact that in both the mean voltage and the spectrum analyzer received power, there are two measurement points that are very close together, leading to a large deviation in the offset that is not visible when plotting the two measurements against each other, as the points overlap in that case. The same effect is also partially visible in the graph of the slope.

The standard deviation of the power detector samples increases at lower power levels. The maximum standard deviation reached is approximately 0.015 V. Again we can translate this to power using the slope, and this becomes 0.5 dBm. If we take as absolute maximum three standard deviations ( $3\sigma$ ), this is a maximum error of 1.5 dBm.

Of the two sources of error in the measurements, the offset at different frequencies is a static error. However, by averaging a number of samples the dynamic error characterized by the standard deviation can be reduced. A mean taken of  $n$  samples will have a new standard deviation calculated according to 5.1. Using this equation, the number of required samples can be found from a stated acceptable error level.

$$\sigma_{\text{sample mean}} = \frac{\sigma}{\sqrt{n}} \quad (5.1)$$

For example, if the error should be reduced below the quantization error of the ADC, which is  $\frac{2.048}{2^{12}} = 500 \mu\text{V}$ , the  $3\sigma$  needs to be lower than that, so the number of samples required is then  $n = \frac{0.015 \cdot 3^2}{500 \mu\text{V}} = 8100$ . When using this method, however, the maximum time allowed for a measurements also needs to be taken into account.

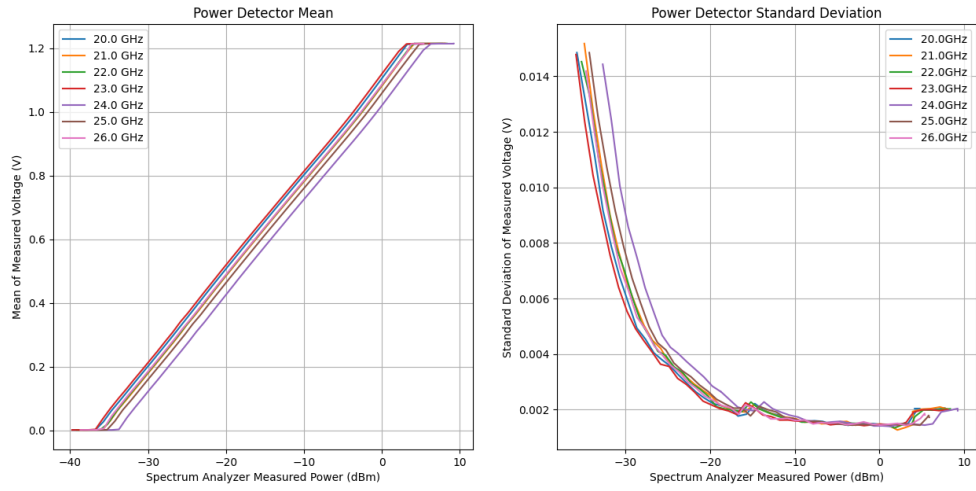


Figure 5.1: Power Detector measurements with direct connection

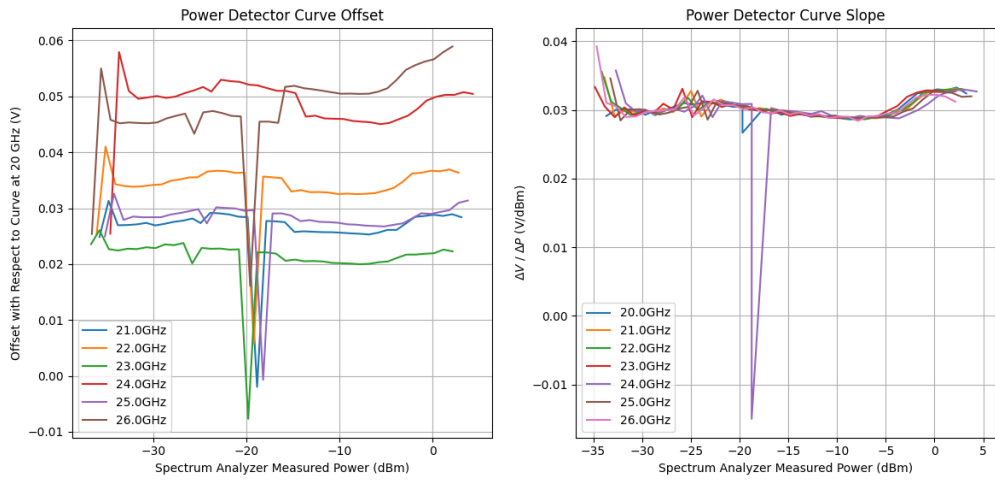


Figure 5.2: Power detector single-tone response slope and offset of mean

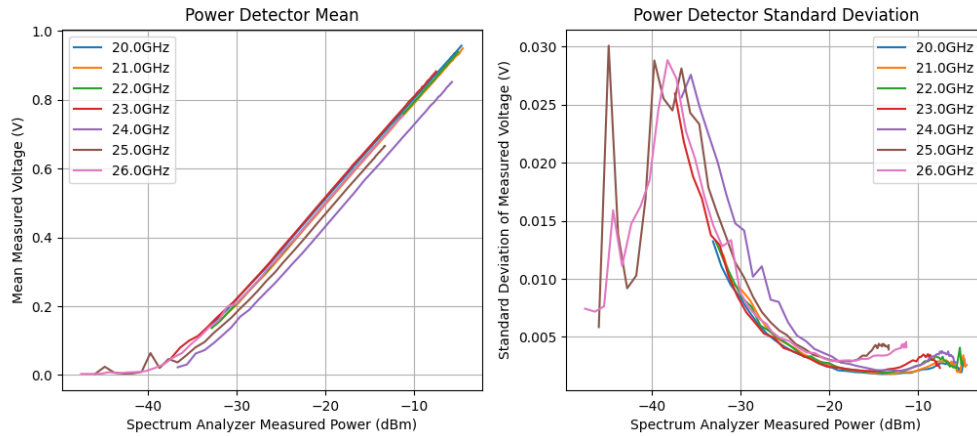


Figure 5.3: Power detector measurements with over-the-air setup

The offsets of the curves might also limit the usefulness of the sensor in cases where the transmit frequency is not known. These offsets are mostly caused by variations in the reflection coefficient of the detector board and the chip, leading to a small difference in the actual power received by the LTC5596 which is constant over power.

## 5.2 Over-the-Air Setup

The measurement setup used for this part can be seen in figure 3.4. With the over-the-air setup the same type of measurements were done as with the direct connection. The mean and standard deviation of the power detector samples are plotted against the received power on the spectrum analyzer in figure 5.3. Again the standard deviation is plotted from slightly higher powers on due to the samples clipping to zero. Even with the amplifier added to compensate the additional losses, the detector does not receive enough power to reach to maximum output voltage. Additionally, as the equipment is operated close to the frequency limits, the gain is not the same at all frequencies. As two received levels are graphed against each other, this is not an issue for the accuracy, but it does limit the range for some frequencies even more.

The mean of the samples still shows a linear relation at the higher power levels, but at lower powers the transition to zero output voltage is not as neat as it is with a direct connection. The offsets between the different curves are also different for this setup than for the direct connection. This is because the attached antennas change the matching conditions slightly, so the variations in reflection coefficient have a slightly different impact.

The standard deviation in the over-the-air setup is approximately twice as high as in the direct connection, about 0.03 mV. This corresponds to a error in power of 0 dBm. The standard deviation being twice as large means that to reduce the error to the same levels as in the calculation done for the direct connection, the number of samples required becomes four times higher for a total of 32 400

## 5.3 Multi-tone Setup

The measurement setup used for this part can be seen in figure 3.6. In the multi-tone setup an additional variable is introduced: the number of tones in the signal. This makes it impossible to show all possible combinations of frequency and tone count in a single graph.

A good representation of the difference in response between frequencies can be seen in figure 5.4. This figure shows the mean and standard deviation of the power detector samples for a signal consisting of 4 tones, but the same pattern was observed for different tone counts. It is clear that the differences in frequency that were observed before are still present.

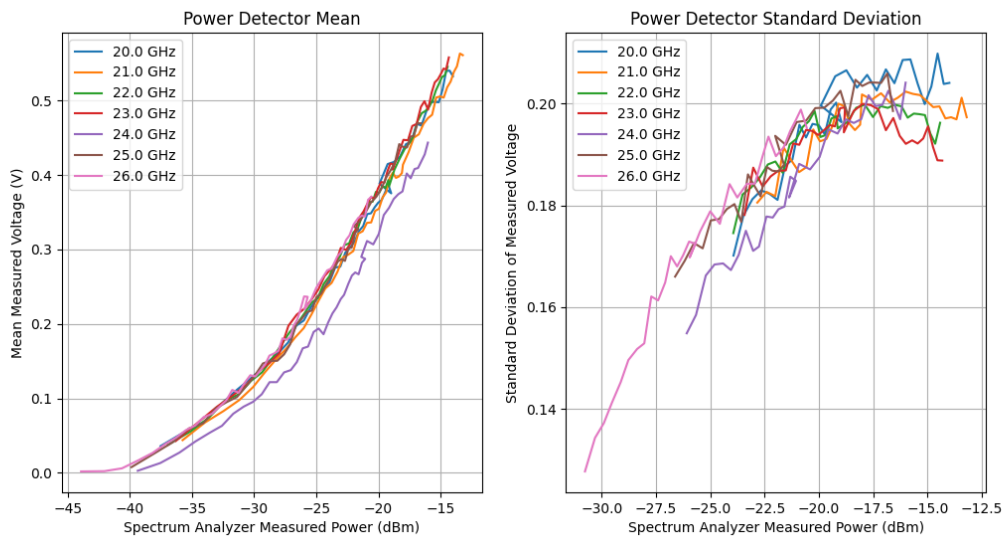


Figure 5.4: Detector response with 4 tones applied for different frequencies

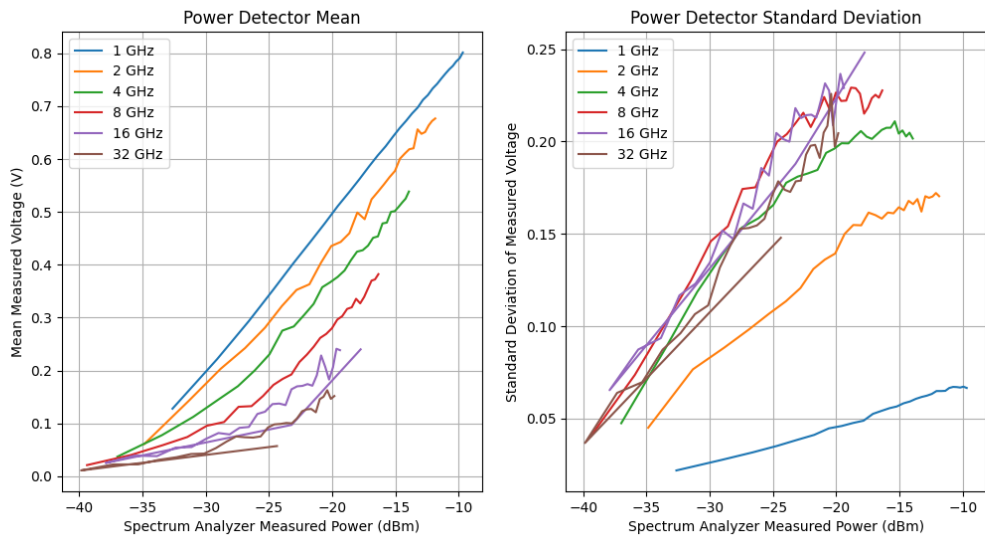


Figure 5.5: Detector response at 20 GHz for different tone counts

It is clear from figure 5.4 that the response is worse than in the single-tone measurements. The mean response is similar to the over-the-air single-tone response in that at low power levels the curves are not linear-in-dB. At higher powers, the response is approximately linear, but even with the average of 2500 samples, the curves are still noisy. The reason for this can be seen in the standard deviation graph, as the standard deviation of the detector output is much larger than in the single-tone setups. In the graph the deviation looks to decrease at lower power levels, however this is again due to the samples being clipped at 0 V. However, as the voltage swings are so large, this effect starts much sooner.

It is also visible that the standard deviation does not decrease as the power levels increase. This points to the source of this noise being different from one having the biggest impact in the single-tone measurements. Indeed the large fluctuations in output voltage with multi-tone excitation are caused by the transient response of the LTC5596 chip and the power fluctuations in the applied signal. In the datasheet [10] it can be seen that the transient response takes 10  $\mu$ s to 20  $\mu$ s, which is about the same duration as that of the modulating waveform.

This behavior is also responsible for the fact that as the number of tones increases, the mean response of the detector for the same applied power level decreases, as can be observed in figure 5.5. The standard deviation in this figure suffers even more from the issue discussed above, as for higher tone counts the mean never becomes high enough to remove the effect of clipping.



# Chapter 6

## Discussion and Conclusion

### 6.1 Conclusion

In the end all mandatory requirements have been fulfilled, however the optional requirement of characterization for QAM-modulated signals was not completed.

The detector board shows a good response to single-tone excitation with the signal connected directly to the power meter. However, different frequencies have slightly different curves, making a wrong readout possible if the transmitted frequency is unknown. With over-the-air single-tone applied to the detector, the response is slightly worse, as the standard deviation of the output voltage is doubled. The mean response is still nicely linear, except for the lowest part of the dynamic range.

For single-tone excitation, the simulation shows that the variation of the output voltage of the power detector in time is mainly dependent on the input noise for lower power levels and the generated noise of the power detector for higher power levels.

With multi-tone excitation applied to the detector the response was quite poor, as the output voltage fluctuations of the detector were very large. Additionally, the mean of these fluctuations was also lower than the mean output voltage with a single-tone waveform of the same power level.

In the end, the current power detector does not seem to be a valid option for the measurement of multi-tone signals, especially as the number of tones increases.

### 6.2 Discussion

The offsets in frequency are difficult to compensate for, as they are caused by the imperfect matching of the LTC5596 chip and once a voltage has been measured it cannot be traced back to a specific frequency. Further investigation is required to better determine the cause of the errors in the response at the multi-tone measurements and how they can be prevented. As the response to multi-tone excitation was less than ideal, it is recommended that the characterization for QAM-modulated signals will also be carried out, as it can now not be guaranteed that the response will be as well-behaved as for single-tone excitation. Additionally, the response for higher frequencies is also not complete, so that would be another possible continuation of the research. Another possible investigation would be if the responses, like the response differences caused by the imperfect matching, differ between multiple LTC5596 boards. Furthermore the simulation could be improved to get a noise simulation that describes the noise behavior in the complete chain. As well as a proper connection between the noise simulation and the Monte Carlo simulation, this has been avoided due to time limitations.



# Appendix A

## Simulation Manual

### A.1 Overview

There are four files for the three setups. Each file consists of another setup and simulation.

- Direct-setup: The simulation of the direct connection setup.
- Direct-multi-setup: The simulation of the direct connection multi-tone setup.
- OTA-setup: The simulation of the over the air connection setup.
- RMSchip: contains the schematic of the power detector.

### A.2 Different Simulators

In each setup there are 6 simulations.

- 'Harmonic balance' needs to be used together with every other option or as a stand alone to simulate the system.
- 'Paramsweep power' and 'Paramsweep frequency' for the power and frequency responses.
- 'Paramsweep power' and 'Monte Carlo analysis' to do monte carlo analysis for multiple input powers.
- 'Noise Controller' to simulate the noise behaviour of the chip.

### A.3 Simulation results

In the simulation results there can be seen the following things:

- The power and frequency response is shown if the 'Paramsweep power' and 'Paramsweep frequency' are enabled. The window can be seen in figure A.1. When the equations of the left or right plot are run with keyboard button 'c' a plot will appear plotted in python. If the plot needs to be edited go to tools -> spyder. At this place the scripts can be found. More explanation can be found in the next section.
- The noise simulation can be seen in figure A.2. The simulation is basically a one time run however sources could be changed to your liking.
- To use the Monte Carlo simulation the user must first decide what he wants. If he wants to simulate the output of the noise it only needs to select N1, N2 and N3 in simulate -> simulation variable settings -> statistics. If the user wants to include the uncertainties he can select more.

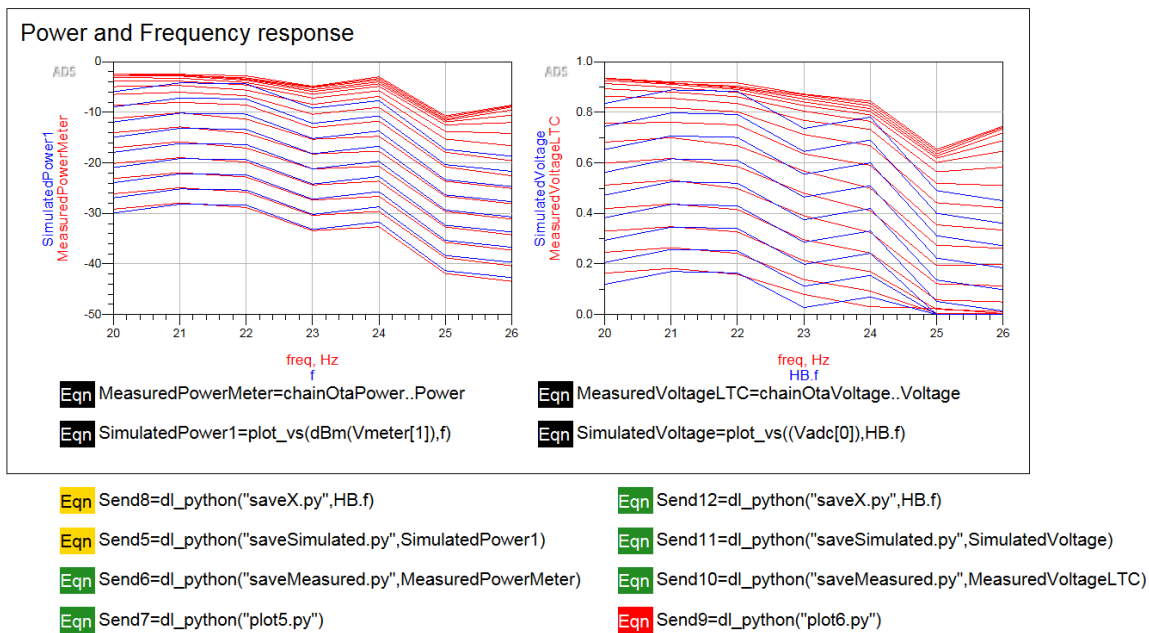


Figure A.1: Example of power and frequency response

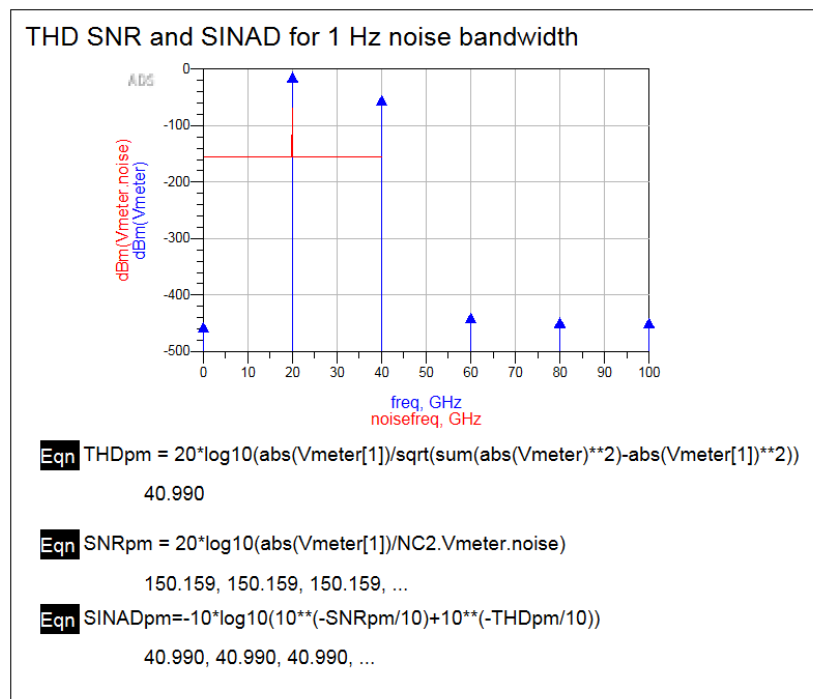


Figure A.2: Example of a noise simulation

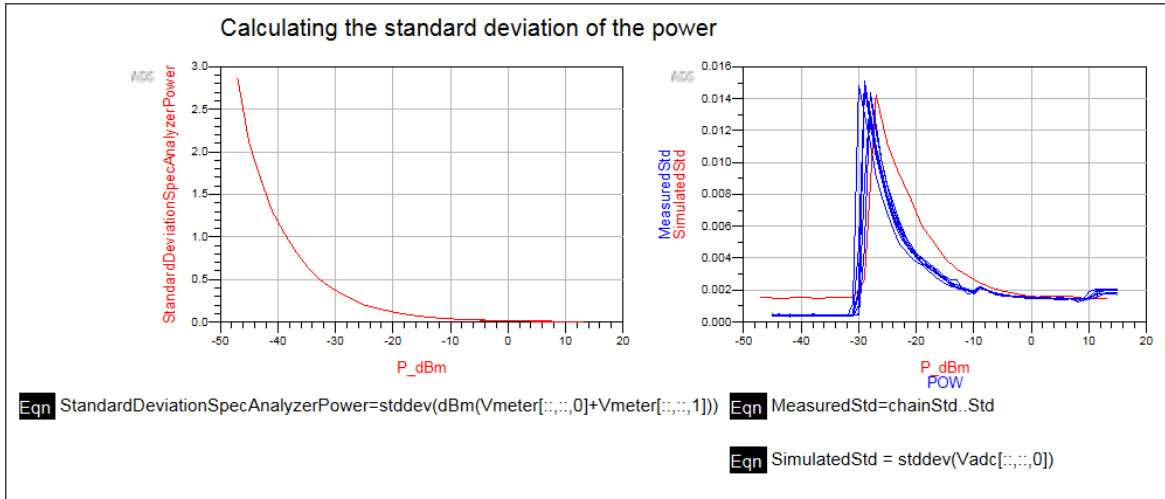


Figure A.3: Example of a Monte Carlo simulation

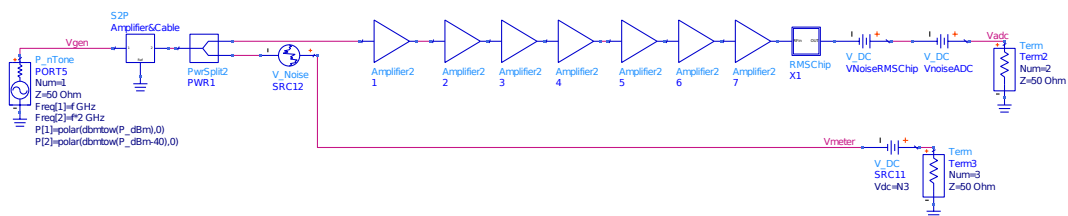


Figure A.4: Schematic for Monte Carlo and noise simulation

## A.4 Addon datalink ADS

With the use of datalink python scripts can be run with an equation. In figure A.5 the equation can be seen. This later will be used for plotting data and simulating the number of iterations needed. This can also be used to plot 3d data or moving data from and to ADS. However this has mostly been used to make nice plots. The major limitations are that it simply adds all the data together in one long list and sends it to python. Sending multiple variables to one script can cost a lot of time to untangle the data. Therefore multiple scripts are run to save the data one by one to a numpy format which are loaded by the plot function.

 `out3=dl_python("stddev_calc.py",dBm(Vmeter[1]))`

Figure A.5: Button to run python script

# Bibliography

- [1] Phase noise background. URL [https://www.ieee.li/pdf/essay/phase\\_noise\\_basics.pdf](https://www.ieee.li/pdf/essay/phase_noise_basics.pdf).
- [2] *Modern RF and Microwave Measurement Techniques*. The Cambridge RF and Microwave Engineering Series. Cambridge University Press, 2013. doi: 10.1017/CBO9781139567626.
- [3] The essential signal generator guide, building a solid foundation in rf – part 1, oktober 2018.
- [4] Erion Bukaçi, Thoma Korini, Erion Periku, Skënder Allkja, and Paulin Sheperi. Number of iterations needed in monte carlo simulation using reliability analysis for tunnel supports. *International Journal of Engineering Research and Applications*, 6:60–64, 06 2016.
- [5] Wei Fan, Jesper Ø. Nielsen, and Gert F. Pedersen. Estimating Discrete Power Angular Spectra in Multiprobe OTA Setups. *IEEE Antennas and Wireless Propagation Letters*, 13:349–352, 2014. ISSN 1548-5757. doi: 10.1109/LAWP.2014.2306205. Conference Name: IEEE Antennas and Wireless Propagation Letters.
- [6] S. I. Ivanov and A. P. Lavrov. Optimal operation modes of low cost RF power diode detector on multi-tone signals. In *2018 International Symposium on Consumer Technologies (ISCT)*, pages 51–53, May 2018. doi: 10.1109/ISCE.2018.8408917. ISSN: 2159-1423.
- [7] Geonho Jang, Seho Park, Hongsik Keum, Sangho Choi, and Goonyeon Kim. Antenna Measurement System for 5G Application. In *2018 International Symposium on Antennas and Propagation (ISAP)*, pages 1–2, October 2018.
- [8] Walt Kester. Understand sinad, enob, snr, thd, thd + n, and sfdr so you don't get lost in the noise floor, October 2008.
- [9] Walt Kester. The good, the bad, and the ugly aspects of adc input noise—is no noise good noise?, 2009.
- [10] *LTC5596 100MHz to 40GHz Linear-in-dB RMS Power Detector with 35dB Dynamic Range*. Linear Technology, 2016.
- [11] H. P. Moyer, J. N. Schulman, J. J. Lynch, J. H. Schaffner, M. Sokolich, Y. Royter, R. L. Bowen, C. F. McGuire, M. Hu, and A. Schmitz. W-Band Sb-Diode Detector MMICs for Passive Millimeter Wave Imaging. *IEEE Microwave and Wireless Components Letters*, 18(10):686–688, October 2008. ISSN 1558-1764. doi: 10.1109/LMWC.2008.2003471. Conference Name: IEEE Microwave and Wireless Components Letters.
- [12] Musters. Real-time 3d characterization of antenna systems, 2019.
- [13] Per Noren, Lars Jacob Foged, Lucia Scialacqua, and Alessandro Scannavini. Measurement and Diagnostics of Millimeter Waves 5G Enabled Devices. In *2018 IEEE Conference on Antenna Measurements Applications (CAMA)*, pages 1–4, September 2018. doi: 10.1109/CAMA.2018.8530472.
- [14] David M Pozar. *Microwave engineering; 3rd ed*. Wiley, Hoboken, NJ, 2005.

- [15] Saad Qayyum and Renato Negra. 0.8 mW, 0.1–110 GHz RF power detector with 6 GHz video bandwidth for multigigabit software defined radios. In *2017 IEEE MTT-S International Microwave Symposium (IMS)*, pages 1722–1725, June 2017. doi: 10.1109/MWSYM.2017.8058975.
- [16] Jiayi Wang, Yongan Zheng, Fan Yang, Fan Tian, and Huailin Liao. A wide band CMOS radio frequency RMS power detector with 42-dB dynamic range. In *2015 IEEE International Symposium on Circuits and Systems (ISCAS)*, pages 1678–1681, May 2015. doi: 10.1109/ISCAS.2015.7168974. ISSN: 2158-1525.
- [17] T. Zhang, W.R. Eisenstadt, R.M. Fox, and Q. Yin. Bipolar Microwave RMS Power Detectors. *IEEE Journal of Solid-State Circuits*, 41(9):2188–2192, September 2006. ISSN 1558-173X. doi: 10.1109/JSSC.2006.880592. Conference Name: IEEE Journal of Solid-State Circuits.
- [18] Ze Zhang, Rajesh Rajavel, Peter Deelman, and Patrick Fay. Sub-Micron Area Heterojunction Backward Diode Millimeter-Wave Detectors With 0.18  $\mu\text{m}$   $\text{pW}/\text{Hz}^{1/2}$  Noise Equivalent Power. *IEEE Microwave and Wireless Components Letters*, 21(5):267–269, May 2011. ISSN 1558-1764. doi: 10.1109/LMWC.2011.2123878. Conference Name: IEEE Microwave and Wireless Components Letters.
- [19] Yijun Zhou and Michael Yan-Wah Chia. A Low-Power Ultra-Wideband CMOS True RMS Power Detector. *IEEE Transactions on Microwave Theory and Techniques*, 56(5):1052–1058, May 2008. ISSN 1557-9670. doi: 10.1109/TMTT.2008.921299. Conference Name: IEEE Transactions on Microwave Theory and Techniques.